Synthesis and Characterization of Fe_3O_4-NPs from Leaves *C. Spinosa* Extracts and their Anti-Microbial Activity

Majid A. Mohaisen[1], Sirhan.M.M[2]

[1]*Department of Chemistry, College of Science, University of Anbar, Iraq.*
[2]*Department of Chemistry, College of Education for Pure Sciences, University of Anbar, Iraq.*
Email: majid.a.m@uoanbar.edu.iq

In this study, Fe_3O_4-NPs were synthesized using green synthesis and coated with different extracts of *C. spinosa* such as water, alcohol, and alkaloids. The goal of this study was to find out how well these nanoparticles zone of inhibition (ZOI) of harmful bacteria gram positive and gram negative such as *Bacillus cereus*, *Staphylococcus aureus, Klebsiella pneumoniae,* and *Pseudomonas aeruginosa*. TEM and FESEM examine nanoscale Fe_3O_4-NP powder size, shape, and surface. FTIR may reveal powder functional groups. Analysis of Fe_3O_4-NP particle structure and composition by XRD. These approaches reveal the substance's atomic and concrete properties. The KBr disc method proved suitable for analysis. Functional groupings in FTIR studies Phenolic molecules in the plant extract caused FTIR peaks in A1, A2, A3, A4, and A5 compounds. These wavenumbers are 3272, 3421, 3417, 3437, and 3371 cm^{-1}. Fe-O Linka appears at 504, 378, 389, 555, and 567 cm^{-1}. The hydroxyl group O-H stretching vibration is crucial to NP synthesis, and these peaks are connected. Green Fe_3O_4-NPs A2 and A4 have C=C and C=O functional group FTIR bands at 1647 and 1743 cm^{-1}. Co-precipitated Fe_3O_4-NPs in A3 and A5 had similar FTIR peaks. Fe_3O_4-NPs' 1643 and 1604 cm^{-1} functional groups may identify synthesis chemicals. A Petri dish disk diffusion experiment examined the antibacterial capabilities of the nanocomposites. We prepared 25, 50, 100, 150, and 200 mg/mL nanocomposites. Alcohol extract inhibited four microorganisms in codes C and C1. Water-loving bacteria behave differently in this zone, making extract-alcohol comparisons important. Strong plant antibacterial tannins and flavonoids only dissolve in alcohol or alcohol mixtures, thereby improving extract efficacy and shelf life. Fluids may stabilize tannins and antimicrobial flavonoids from clean and alcohol-binary extractions.

Keywords: Fe_3O_4-NPs, green synthesis, co-precipitation, *C. spinosa*, Anti-Microbial, ZOI, Petri dish.

1. INTRODUCTION

The *Capparaceae* family comprises 700 species in 40-50 groupings. Horticultural and economic recognition is low for the members. Most species live in subtropical and tropical regions, except in the Mediterranean and America. About 15 species of this plant thrive in desert Africa.[1] It is also antiviral, antibacterial, anticancer, antidiabetic, and antioxidant. The plant is known for its cleansing, restricting, and anti-inflammatory properties.[2] Metal nanoparticles have more surface area. Nanomaterials' size, surface characteristics, interfacial behaviour, and quantum phenomena determine their physical and chemical properties. Medicine, biology, and engineering use nanoscale metals.[3] Ag NPs inhibit Gram-positive and Gram-negative bacteria growth and function. Ferrous nanoparticles (Fe-NPs) remove organic debris, ions, and media-polluting pigments well. Furthermore, they inhibit germ growth.[4] Fe-NPs can effectively remove organic, metallic, and non-metallic ions and dyes from matrices. In addition, they hinder microorganism development.[5] Both chemical and mechanical methods are available for synthesizing metal NPs. These processes require the use of energy and dangerous substances. Consequently, there is a need for the advancement of environmentally sustainable metallic nanoparticles. This is achievable using biological resources. For many years, plants, algae, fungi, bacteria, and viruses have demonstrated the ability to generate low-cost, energy-efficient, and safe metallic NPs.[6] Green synthesis outperforms chemical and physical methods in sustainability, economy, safety, and environmental friendliness.[5] Synthesis procedures that are innovative, cost-effective, ecologically friendly, and productive are increasingly using biological methods. Research on plant extracts that create nanoparticles and lower metal ions is ongoing. Nanostructures in the industry require size and shape precision.[7] The primary determinant of a nanoparticle's features Some examples of analytical procedures are as follows: The FTIR spectra of Fe_3O_4-NPs extract may be used to identify the characteristic peaks of Fe_3O_4-NPs. In addition, other techniques such as transmission electron microscopy (TEM), powder X-ray diffraction (Powder XRD), and field emission scanning electron microscopy (FE-SEM) can also be used.[8] Leaves, vegetables, and roots contain phytochemicals that help plants grow, defend, and endure. They prevent sickness. Plant extracts include main and secondary components. Terpenoids, alkaloids, flavonoids, and phenolics are secondary metabolites; chlorophyll, proteins, and carbohydrates are primary.[9] Antibacterial phytochemicals may prevent illness by reversing cell and epigenetic changes. Additionally, it treats medical issues.[10] Both *in vitro* and *in vivo* investigations can be used to examine biological activity. Significant or catastrophic consequences are expected because of the dosage-dependent nature of biological activity. Metabolism, excretion, distribution, and absorption affect biological activities.[11] Antimicrobial development is essential to fight resistance. Therapeutic antimicrobial medicines have prompted substantial research on NPs. [12] Iron oxide is a good NP because it is abundant, cheap, and involved in many biological processes. Thus, it is ideal for. A better knowledge of NPs might revolutionize nanomedicine by allowing non-toxic chemotherapy and lowering drug-resistant microorganisms. This study tested pathogenic, Gram-positive, and Gram-negative bacteria. This study used a microscope to detect the inhibitory zone of *C.*

spinosa leaf nanocomposites.

2. AIMS AND OBJECTIVE

2.1. Plant material

AL-Baghdadi, Anbar, Iraq, was the site of *Capparis* plant leaf harvests in May and June 2022. The University of Anbar Desert Studies Centre categorised it. After removing pollutants, the plant was permitted to dry naturally in a cool, shaded place at the surrounding temperature until its weight stabilised. Airtight, opaque containers held the object until removal.

2.2. Chemicals

The experiment utilised iron (II) nitrate hexahydrate (Fe $(NO_3)_2$. $6H_2O$), along with several reagents: 100 µL of dimethyl sulphide (Sigma-Aldrich) at 100% concentration, ethanol at both 100% and 60% concentrations, a 3% solution of sulfuric acid (H_2SO_4) from BDH, 25% ammonium hydroxide (NH_4OH) from Fluka, and deionized water. All of these compounds were acquired from Sigma-Aldrich.

2.3. Preparation of the Extract (crude) from *C. Spinosa*

This experiment followed the procedures with minor changes. The plant extract was obtained from caper leaves. These leaves were collected, rinsed, dried, and ground into a powder using an electric mixer. Sieving removed all suspended particles. Add 200 mL of deionized water to a beaker containing 10 g of powder. A magnetic stirrer stirred the mixture throughout. Heat the mixture at 80°C for 30 min to obtain the brown extract, then cool it. Solution filtration followed. The plant extract reduces the solution in a glass vial at room temperature.[13]

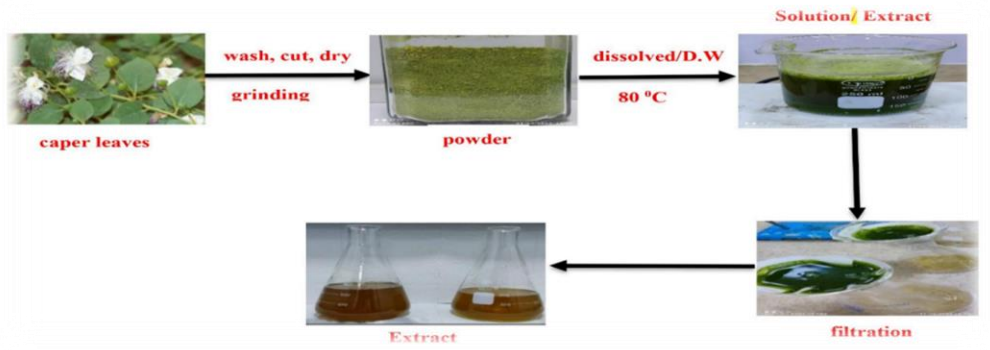

Figure 1: Schematic diagram of preparation of the *C. Spinosa* extract

2.4. Preparation of various extracts from *C. spinosa.*

2.4.1. Water Extract (WE)

Following the procedure described by Pin-Der and Gow-Chin, [14] the plant was extracted using, specifically, 10 g of *capers* combined with 300 mL of boiling deionized water and left to sit for 30 min on a magnetic stirrer. The extract was purified using a Buechner funnel and vacuum-sealed Whatman No. 1 filter paper. Subsequently, it was heated at 60 °C in a rotary

evaporator to concentrate it into 20 mL of extract. The concentrated extract was carefully transferred into a Petri dish and dried in an electric oven at 40 °C for 24 hr. Collect the dried powder, carefully transfer it into sterile bottles, and store it in a cool place until required.

2.4.2. Alcoholic Extract (EE)

The extraction was performed using the method described by Zhou *et al*.,[15] in which 10 g of *capers* powder was extracted with 100 mL of ethanol concentration (60%) and left for 2 h on a magnetic stirrer, filtered by a Buechner funnel with vacuum through Filter paper (Whatman No.1), and the extraction was repeated three times for 2 h each time. The filtrate was collected and concentrated in a rotary evaporator at 50 °C until the volume reached 20 mL, after which the concentrated extract was put onto a Petri dish and dried in an electric oven at 40 °C for 24 h. Scoop the dried powder into clean, dry bottles and store in the refrigerator until needed.

2.4.3. Alkaloid Extract (AE)

The extraction was carried out using the method described by Doncheva *et al.,*[16]in which 10 g of *capers* powder was extracted with 100 mL of (3%) H_2SO_4 solution and placed on a magnetic mixer for 2h The filtrate was passed through a Whatman No. 1 filter paper using a Buechner funnel under vacuum. Next, 25% of a solution of NH_4OH was added gradually until the pH level reached 9–10. The mixture was then concentrated using a rotary evaporator. The concentrated extract was poured into a Petri dish and carefully placed in an electric oven set at 40 °C for drying. Transfer the dried powder into sanitised bottles and keep it refrigerated until it is required.

2.5. Green synthesis of iron oxide nanoparticles (Fe_3O_4)

This experiment was conducted with slight modifications, as described elsewhere. Using a magnetic stir bar, dissolve 2.2 g of aqueous iron (II) nitrate ($Fe(NO_3)_2 . 6H_2O$) in 200 mL of deionized water in a beaker. Next, carefully add 20 mL of the plant extract prepared in step 2.3. Use a burette to add the extract gradually, drop by drop, while continuously stirring the solution at a temperature of 20°C. Then, raise the temperature of the solution to 80°C and adjust the pH by adding 1 M sodium hydroxide (NaOH). This will cause a brown precipitate to form, as shown in the figure below. Allow the precipitate to cool to room temperature, then centrifuge it at a rate of 1,200 rpm/min to remove any remaining fibres filter it using filter papers, and wash three times in deionized water and absolute ethanol to get rid of impurities, and then dry by oven at 60 ^{0}C for 2 hr.[13]

Figure 2: Schematic diagram of green synthesis of Fe_3O_4-NPs of *C. Spinosa*

2.6. Preparation of Fe_3O_4-NPs by co-precipitation method.

Two substances, weighing 24 g and 12 g respectively, were combined in a 2:1 molar ratio. Aqueous solutions containing the Fe^{2+} and Fe^{3+} ions were prepared using deionized water. The mixture was subsequently heated to a temperature of 50 °C for 10 minutes. Next, the mixture was consistently stirred on a magnetic stirrer at 50 °C while being precipitated by ammonia solution. The iron oxide precipitated and produced particles that had a dark hue. Following that, the particles underwent multiple washes with deionized water (2X50 mL) and ethyl acetate (2X50 mL) after being separated from the solution using a strong magnet. The powder was dried overnight at 100 °C in a hot air oven.[17]

$$\mathbf{FeCl_2.4H_2O + 2FeCl_3.6H_2O + 8NH_4OH \rightarrow Fe_3O_4 + 8NH_4Cl + 20H_2O}$$

2.7 Preparation of several extracts of *C. Spinosa*, coated -Fe_3O_4 NPs.

According to the co-precipitation procedure described in previous publications, with minor modifications, to produce composites of Fe_3O_4 coated with *Capparis* extracts (CEs)-coated Fe_3O_4 composites. This method is available in other sources.[18] Initially, 1 g of *C.* extract and 0.5 g of Fe_3O_4 were dissolved in a beaker containing 50 mL of deionized water. Afterwards, they were promptly incorporated into the solution to increase the pH to around 10. The procedure was executed with utmost expertise, guaranteeing its successful completion at room temperature while maintaining continuous stirring for 24 h. The Fe_3O_4-*C.* Es composite was synthesised and recovered by magnetically separating the product after ultrasonic dispersion. Afterwards, the nanocomposites underwent several rinses with deionized water and were then dried under vacuum conditions at room temperature Table 1 describes the nanocomposites as codes.

Table 1: Name of nanocomposites used in the study

Name of Samples	***Code***
Fe_3O_4-NPs only co-precipitation method	A
Fe_3O_4-NPs-coated crude (C. spinosa)	B
Fe_3O_4-NPs-coated ethanol extract	C
Fe_3O_4-NPs-coated coated water extract	D
Fe_3O_4-NPs-coated alkaloid extract	E
Fe_3O_4-NPs- only (green synthesis)	A1
Fe_3O_4-NPs-coated crude (C. spinosa)	B1
Fe_3O_4-NPs-coated ethanol extract	C1
Fe_3O_4-NPs-coated water extract	D1
Fe_3O_4-NPs-coated alkaloid extract	E1

3. Characterization of Fe_3O_4-NPs:

The primary objective of these measurements is to ascertain the shape, morphology, and structure of the synthesised nanomaterials. The change in the solution colour in the reaction mixture was visually observed. The colour shift suggests the presence of *C.* nanoparticles. The measurement was conducted using FTIR to identify the functional groups present in Fe_3O_4-NPs. FTIR can record IR absorption spectra. The frequency range is 400–4000 cm^{-1}.[19] The production and crystallinity of Fe_3O_4-NPs were confirmed by powder diffraction using an Ultima IV X-ray diffractometer (Rigaku, Inc. in Japan. A transmission electron microscope (TEM) located in Hillsboro, OR, USA, with an accelerating voltage of 200 kV, was used to assess the size and shape of the synthesised Fe_3O_4-NPs. Images of biosynthesized nanoparticles and field emission scanning electron microscopy (FESEM; JEOL-JSM-7600F) are commonly employed techniques for analyzing the morphology and topography of samples. [20]

4. Study of the biological activities of nanocomposite extracts of *C. spinosa* leaf.

In this study, various isolates of microorganisms were utilised, including pathogenic bacteria, Gram-positive bacteria such as *Bacillus cereus* and *Staphylococcus aureus*, as well as Gram-negative bacteria like *Pseudomonas aeruginosa* and *Klebsiella pneumoniae.* These microorganisms were employed as test organisms to assess the inhibitory zone of nanocomposites derived from *C. spinosa* leaves. Identifying the sources of microorganisms used in detecting the inhibitory zone for these particular isolates of microorganisms.

4.1. Evaluation of the sensitivity of microbes to nanocomposite samples.

The effectiveness of the nanocomposites in preventing the growth of the bacterial isolates was assessed using the disk diffusion technique, which was performed on a Petri dish.

4.2. Preparation of nanocomposite discs

The concentrations of the nanocomposites 25, 50, 100, 150, and 200 mg/mL were prepared from Tables 1, where for each of the above concentrations, 50 disks of filter paper with a diameter of 6 mm were prepared in clean glass tubes, autoclaved for 15 min, and then 1 ml of

the above solutions was added to them, shaken using a mixer, for the material to be distributed evenly on the disks. The disks were dried by placing them in an incubator at 40 ^{0}C for 48 h. The imipenem-10µg was the control sample. The test was carried out according to Kirby-Bauer. [21]

4.3. Muller-Hinton agar:

Mueller-Hinton agar is thought to be the best medium to use when testing bacteria's sensitivity to drugs. This study utilised a Hi-Media medium and established it according to the guidelines provided by the manufacturer. A mixture of 38 g of Mueller-Hinton agar and 1 litre of deionized water was prepared. Heat the mixture, stirring regularly, until the powder is fully dissolved. Then, place it in an autoclave at 121°C and a pressure of 1.5 psi for 15 min. The sterile media was poured into Petri dishes at a rate of 20 mL per dish and allowed to solidify at room temperature. The dishes were incubated at 37 °C for 24 hr to ensure a contamination-free environment and eliminate excess moisture. The dishes were stored in the refrigerator until they were needed. [22]

4.4. Spread of discs:

The nanocomposite disks prepared in step 4.2 were carefully placed on the disk surface using forceps, applying gentle pressure. A minimum distance of 24 mm was maintained between each disk. This was done to prevent any interference between the inhibition areas. The dishes were placed upside down and incubated at 37 °C for 24 h.[22]

4.5. Measurement of the inhibition zone:

The diameter of each disc is measured with meticulous accuracy using a millimetre ruler. The measured zone encompasses the entire transparent area surrounding the antibiotic disc, including the disc itself. The clear area indicates the extent to which the antibiotic is preventing bacterial growth as it spreads.[23]

5. Result and discussion

5.1: FTIR spectral analysis

An IR-Prestige-21 Shimadzu FTIR spectrophotometer was used to examine the Fe_3O_4-NPs. The results showed clear absorption bands. This may confirm the successful synthesis of the NPs. The third spectra are shown in Figure 3. They are crude *C. spinosa* (A1), Fe_3O_4 by green synthesis (A2), and Fe_3O_4-coated *C. spinosa* by green synthesis (A3). The KBr disc process was selected for analysis because of its suitability.The spectra visually represent the different processes involved in each synthesis method. By carefully examining the FTIR spectrum of an extract of Fe_3O_4 NPs, it is possible to quickly identify the distinct peaks that belong to Fe_3O_4 NPs.[20] Figure 3 shows the FTIR spectra of *C. spinosa* and Fe_3O_4-NPs prepared using various methods. The peaks observed in the FTIR spectrum, specifically at wavenumbers in (A1, A2, and A3), are 3272, 3421, and 3437 cm^{-1} respectively, are believed to be caused by the presence of the phenolic molecule in the plant extract. The peaks observed here are associated with the stretching vibration of the hydroxyl group O-H, which plays a significant role in the synthesis of NPs.[24] The FTIR spectra of the green Fe_3O_4-NPs in (A2 and A3) show peaks at 1647 and 1743 cm^{-1}, indicating the presence of stretching bands for the C=C and C=O functional groups,

respectively. The presence of functional groups at wave numbers 1643 and 1604 cm^{-1} in Fe_3O_4-NPs can help identify the organic constituents likely used in the synthesis process. The provided data showcase the crucial absorption bands associated with the Fe–O bonds, specifically at wavenumbers 504, 378, 389, 555, and 567 cm^{-1} in (A1, A2, A3, A4, and A5), respectively.[25] The absorption bands observed indicate a thorough analysis of the crystal structure of the Fe_3O_4-NPs. In addition, the existence of these particular infrared absorption bands suggests the presence of Fe-O bonds in both the tetrahedral and octahedral sites. The spinel structure of the Fe_3O_4-NPs is solidified in their pure form.[26] The spectra of magnetite nanoparticles, whether prepared using environmentally friendly methods, and through co-precipitation, or coated with *C. spinosa* extracts, all exhibit the presence of four distinct bands at 1542, 1539, 1550, 1558, and 1361 cm^{-1}, as shown in Figure 3. The bands are a result of the stretching vibrations in the carboxyl group COO, which occur asymmetrically and symmetrically. The bands observed at wavenumbers 2851, 2934, 2916, 2769, and 2924 cm^{-1} in Figure 3: (A1, A2, A3, A4, and A5) are a result of the asymmetric and symmetric stretching vibrations of the CH_2 groups found in the coating agents.[27] Confirms the effective bonding between the organic coating agents and the nanoparticles.

Wavenumber cm^{-1}

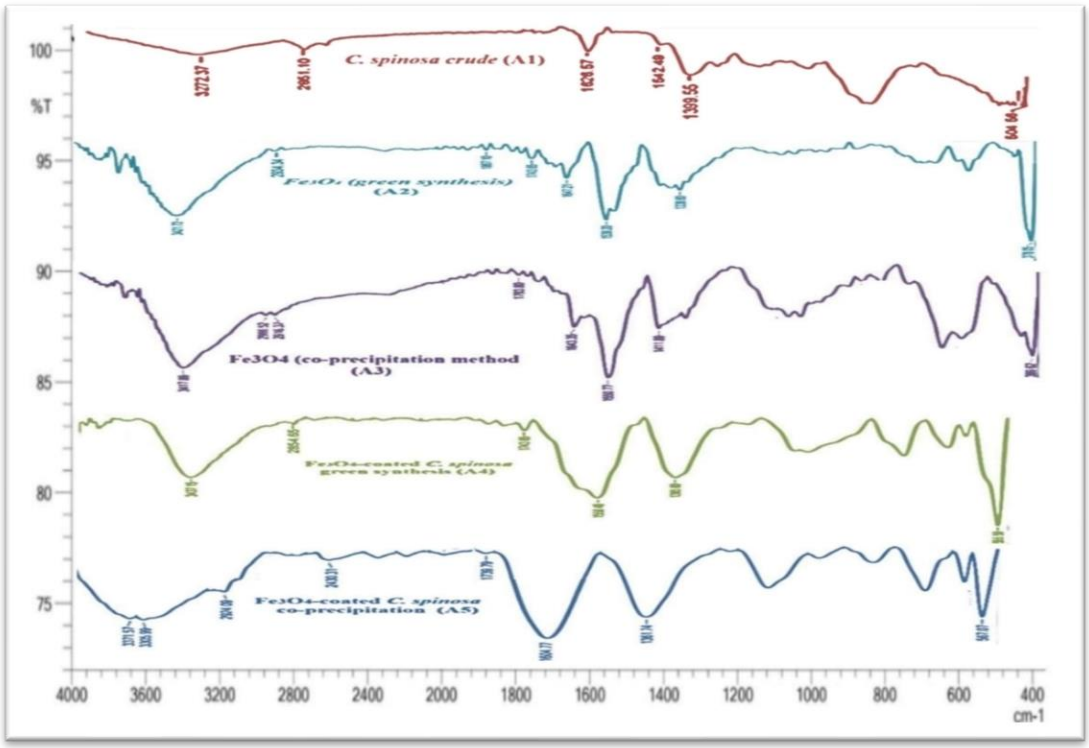

Figure 3: FTIR spectrum of crude *C. spinosa* in (A1) and Fe_3O_4-NPs synthesized from *C. spinosa* green synthesis in (A2), Fe_3O_4-NPs prepared by the co-precipitation method in (A3), Fe_3O_4-NPs coated *C. spinosa* (crude) by green synthesis in (A4), Fe3O4-NPs coated C. spinosa (A5)

5.2. Transmission electron microscopy (TEM)

Understanding the shape and size distribution of nanoparticles is crucial for evaluating their potential applications in various fields, such as medicine, electronics, and environmental research. Figure 4 (a and b) displays the TEM image and size distribution, respectively. Figure 4a illustrates the production of *C. spinosa* extracts using green synthesis, which yields Fe_3O_4-NPs with remarkably consistent sizes. It is important to mention that there are aggregates found in various regions of this sample. Furthermore, it is stated that all of the particles have a spherical or cubic shape. In addition, Figure 4b demonstrates the process of preparation using the chemical technique known as the co-precipitate method. In Figure 4a, the analysis of the particle size distribution curve of Fe_3O_4-NPs revealed that the average diameter of these nanoparticles was found to be approximately 8.9 nm, with a standard deviation of 2.26. On the other hand, the size's average standard deviation is 9.2 nm, as depicted in Figure 4b, with a value of 2.8. On the other hand, when two different production procedures were used, coated Fe_3O_4-NPs containing extracts of *C. spinosa* were produced. So, noticed slight modifications in both form and size distribution. This discovery is in line with the previous (FTIR) data presented in Figure 3. The size distribution can be observed in Figure 5 (a1 and b1). The average diameter of the Fe_3O_4-NPs encapsulated through the process of green synthesis Figure 5 (a1) is 11.2 nm, with a standard deviation of 3.2. It is worth mentioning that the average diameter of the Fe_3O_4-NPs coated using the co-precipitation method in Figure 5 (b1) is 11.5 nm, with a standard deviation of 3.7.[28] After the application of a coating with *C. spinosa* extract, it was analysed via the use of TEM and the image editing software ImageJ that the particle size demonstrated an increase.[29] The Fe_3O_4-NPs, which were subsequently synthesised with extracts of the *C. spinosa* plant, were accomplished by the utilisation of these two distinct methods; Table 2 that follows gives more clarification into this matter.

Table 2: Size of Fe_3O_4-NPs green and co-precipitation methods

Type of iron oxide	**mean**	**St.dev.**	**minimum**	**medium**	**maximum**
Fe_3O_4-NPs green synthesis	8.9	2.26	4.15	9.17	14.5
Fe_3O_4-NPs co-precipitation	9.2	2.8	4.5	9.5	17.9
Fe_3O_4-coated extract *C.sp* green	11.2	3.2	6.3	10.5	22.5
Fe_3O_4-coated extract *C.sp* co- precipitation	11.5	3.7	6.8	10.7	23.7

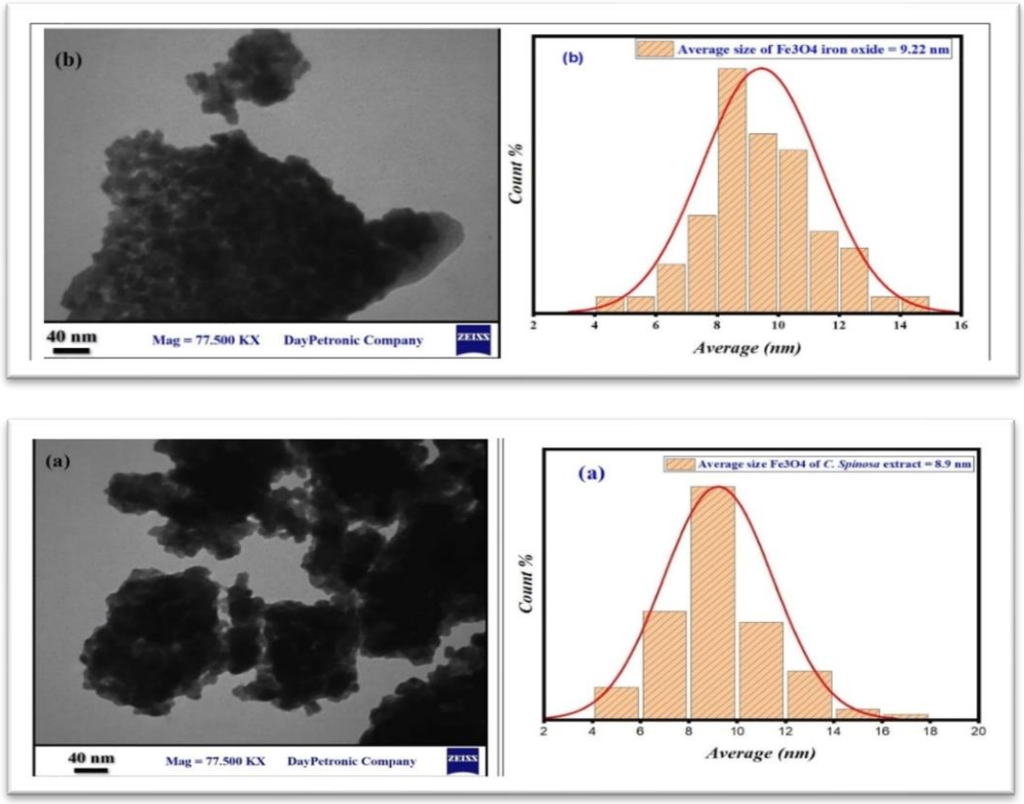

Figure 4: TEM images (a) Fe_3O_4 of green and (b) Fe_3O_4 of co-precipitation methods

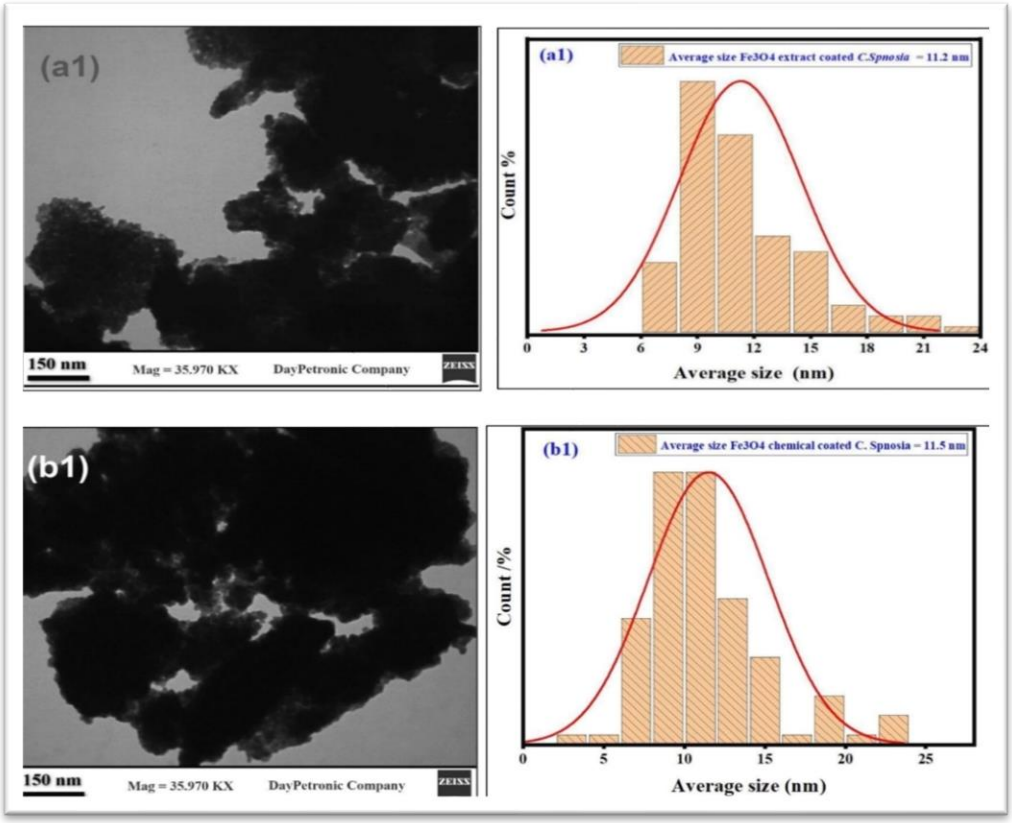

Figure 5: TEM images (a1) Fe_3O_4-coated of *C. Sp. extract* by green synthesis and (b1) Fe_3O_4-NPs- coated *C. Sp.* extract by co-precipitation method.

5.3. Field emission scanning electron microscopy (FESEM)

The Fe_3O_4-NPs were examined using FESEM. A small quantity of the sample was carefully placed on a carbon-coated copper matrix to create a thin film. The excess solution was meticulously removed using blotting paper, and the film on the FESEM grid was left to dry by placing it under a mercury lamp for 5 min. State-of-the-art imaging techniques were used to analyse the structural features. The analysis of the FESM results showed that the Fe_3O_4-NPs produced had a shape that was almost perfectly spherical and uniform. The consistent size and shape of the nanoparticles play a crucial role in determining their magnetic properties and suitability for various applications.[30] The study conducted on the Fe_3O_4-NPs found that they exhibited a predominantly spherical shape and were evenly distributed in terms of size. Fe_3O_4-NPs exhibit a nearly spherical morphology, which is crucial for their magnetic properties and practical applications. This observation suggests that the nanoparticles have a consistent size and shape, which enhances their magnetic properties and potential uses.[31] The Fe_3O_4-NPs produced had average sizes of 24.6 nm and 25.04 nm, respectively, as shown in Figure 6 (a and b). The Fe_3O_4-NPs displayed a consistent distribution upon examination with (FESEM), showcasing a nearly spherical form.[32] The majority of the synthesised Fe_3O_4-NPs displayed a predominantly spherical shape, with their size falling within the nanoscale range as

determined by measurement, as indicated in Table 2. A green synthesis method was employed to coat extracts of *C. Spinosa*, along with Fe_3O_4-NPs coated extracts of *C. Spinosa* using the co-precipitation method. In Figure 7 (a1 and b1), the average size of the NPs was determined to be 27.3 nm and 27.5 nm, respectively. There is evidence of an enlargement in the Fe_3O_4-NPs, which aligns with the findings from the FTIR and TEM methods. Displaying these findings are Figure 7 (a1 and b1). The nearly spherical shape of Fe_3O_4-NPs is highly significant for their magnetic properties and the numerous applications in which they are utilised. Various synthesis approaches can be utilised to achieve the desired shape modification in the model.

Table 2: Size of Fe_3O_4-NPs green and co-precipitation methods

Type of iron oxide	**mean**	**St.dev.**	**minimum**	**medium**	**maximum**
Fe_3O_4-NPs green synthesis	**24.6**	**5.7**	**9.9**	**25**	**41.3**
Fe_3O_4-NPs co-precipitation	**25.04**	**6.8**	**10.9**	**25.3**	**45.4**
Fe_3O_4-coated extract *C.sp* green	**27.3**	**7.5**	**11.5**	**26.7**	**50.5**
Fe_3O_4-coated extract *C.sp* co-precipitation	**27.5**	**7.5**	**11.9**	**26.6**	**53.9**

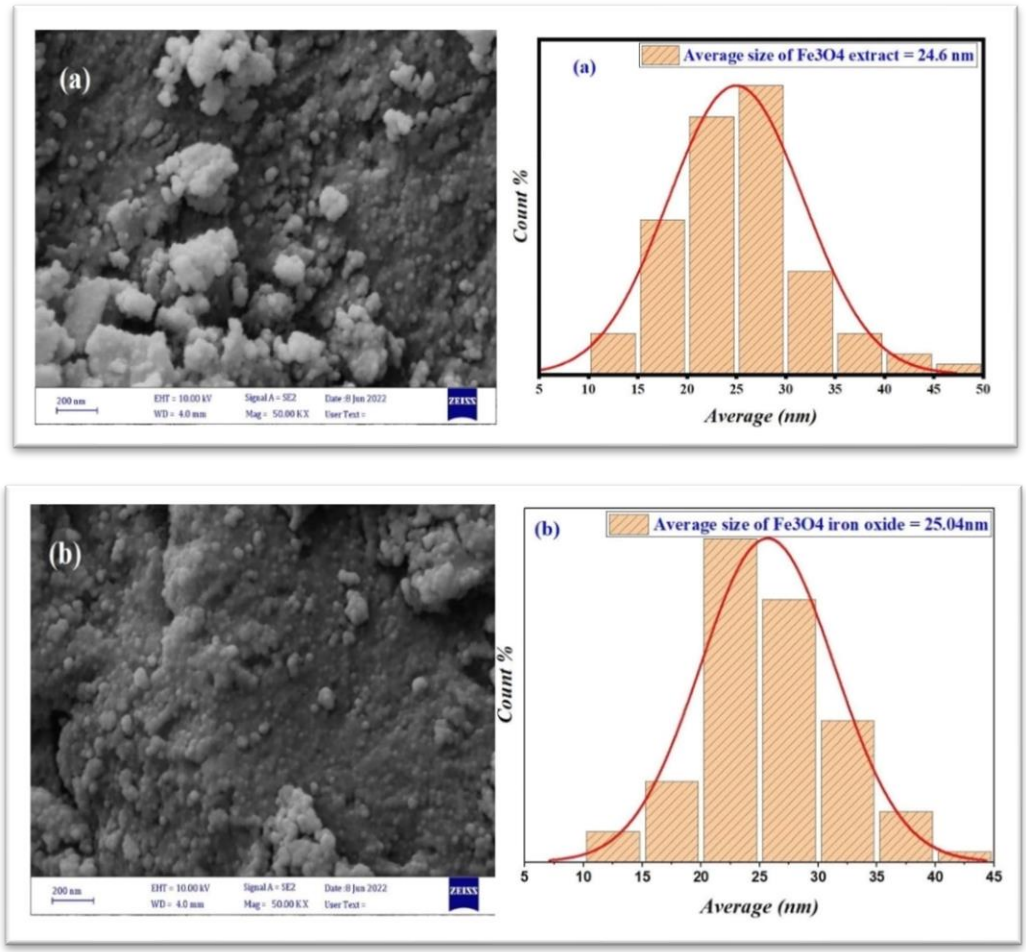

Figure 6: FESEM image (a) Fe_3O_4 of green and (b) Fe_3O_4 of co-precipitation methods.

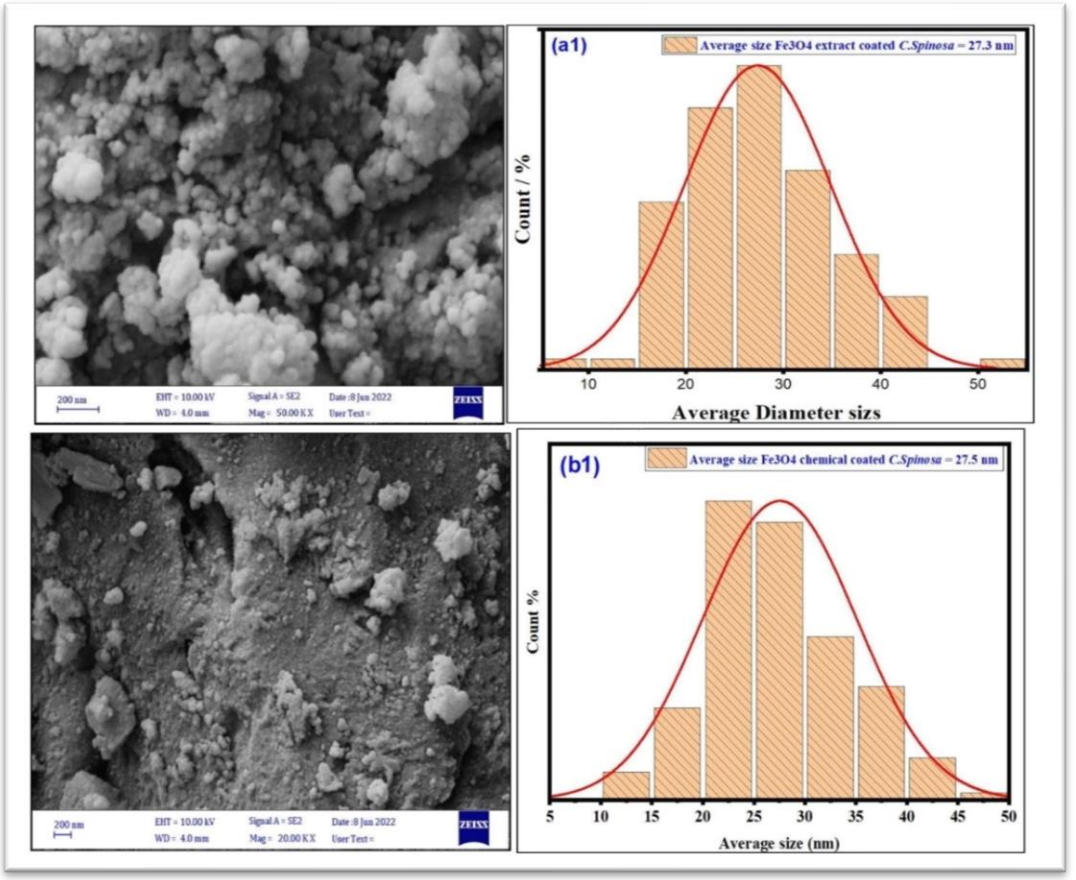

Figure 7: FESEM images (a1) Fe_3O_4-coated of *C. Sp. extract* by green synthesis and (b1) Fe_3O_4-NPs- coated *C. Sp.* extract by co-precipitation method.

5.4. X-ray diffraction (XRD) analysis

Crystalline materials may be identified and NPs forms can be characterised using a process known as XRD, which does not damage the material being affected.[33] This device is used to measure the ratios of crystalline substances and identify extremely small minerals such as NPs and nano-clays. The Scherrer equation has been widely employed to characterize various metal NPs such as hematite, maghemite, and magnetite. This equation is commonly employed to calculate the average crystallite size.[34]·[35] $d = k\lambda/(\boldsymbol{\beta}\cos\boldsymbol{\theta})$ ……. (1)

In the above equation, the symbol "d" represents the particle size, "k" denotes the Sherrer constant with a value of 0.9, "λ" represents the X-ray wavelength with a magnitude of 0.15406 nm,"$\boldsymbol{\beta}$" signifies the breadth of the XRD peak at half-height, and "θ" represents the Bragg diffraction angle. Figure 8 (a and b) X-ray diffraction patterns of Fe_3O_4-NPs synthesized using *C. spinosa* extract using green synthesis and co-precipitation methods.[36] Notable diffraction peaks were discovered, characterised by $2\boldsymbol{\theta}$values of 30.30, 35.60, 43.30, 53.90, 57.30, 62.90, and 74.50. The values can be found within the specified range. The crystal planes offer

valuable insights into the atomic configuration of the Fe_3O_4-NPs generated using these procedures. When evaluating the physical and chemical properties of NPs, the (220), (311), (400), (422), (511), (440), and (533) planes are extremely useful. These results indicate that magnetite NPs possess a spinel phase structure that aligns with the established XRD standard for magnetite.[37] This study highlights a strong correlation between peak widening observed in (XRD) and the particle size. The average size of the magnetic Fe_3O_4-NPs generated using the green synthesis approach was 7.72 nm Figure 8a, whereas the co-precipitation process yielded an average size of 8.9 nm Figure 8b. In the XRD analysis, a peak with a higher intensity signifies a larger concentration of the mineral or molecule being studied, as shown in Figure 8. In addition, the difference in NPs size in the current study is consistent with the results obtained by FTIR, TEM, and FESEM.

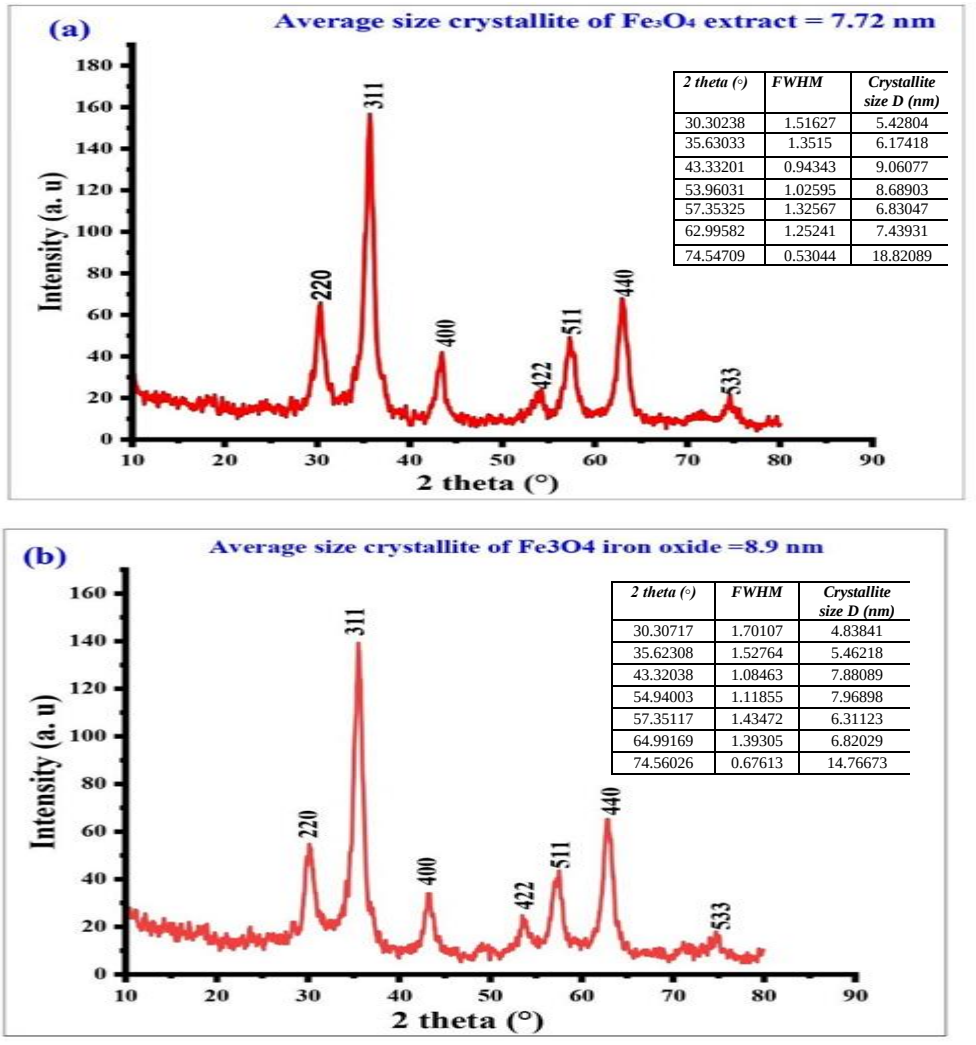

2 theta (°)	*FWHM*	*Crystallite size D (nm)*
30.30238	1.51627	5.42804
35.63033	1.3515	6.17418
43.33201	0.94343	9.06077
53.96031	1.02595	8.68903
57.35325	1.32567	6.83047
62.99582	1.25241	7.43931
74.54709	0.53044	18.82089

2 theta (°)	*FWHM*	*Crystallite size D (nm)*
30.30717	1.70107	4.83841
35.62308	1.52764	5.46218
43.32038	1.08463	7.88089
54.94003	1.11855	7.96898
57.35117	1.43472	6.31123
64.99169	1.39305	6.82029
74.56026	0.67613	14.76673

Figure 8: XRD images (a) Fe_3O_4-NPs by green and (b) Fe_3O_4-NPs by co-precipitation methods.

5.5. Evaluation of the sensitivity of microbes for nanocomposite samples.

Fe_3O_4-NPs, which were prepared by green and co-precipitation methods and coated with different extracts such as (water, alcoholic, and alkaloids) are used to assess the inhibition zone of the harmful bacteria and other microorganisms used in this study. The antimicrobial efficacy of nanocomposites was evaluated using a disc diffusion assay in a Petri dish. Nanocomposites were synthesised at concentrations of 25, 50, 100, 150, and 200 mg/mL using the samples specified in Table 1. The resulting material was evaluated to establish its antibacterial effectiveness against *Bacillus cereus (a), Staphylococcus aureus (b), Klebsiella pneumoniae (c),* and *Pseudomonas aeruginosa* (d) using the agar disc-diffusion method. Figure 9 demonstrates a significant area where bacterial growth is inhibited (zone of inhibition, ZOI) at different dosages. The most effective concentration of ZOI was determined to be 100 mg/mL, as seen in Figure 10 for both the green and co-precipitation methods. Hence, the chemical displays antibacterial properties that specifically affect microorganisms, leading to a reduction in the rate of bacterial growth as the number of NPs increases. Put simply, the more of the chemical there is, the more effective it is in getting rid of bacteria. NPs have bactericidal activity against both gram-positive and gram-negative bacteria, including *Klebsiella pneumoniae* and *Staphylococcus aureus*.[38] Iron oxides at the nanoscale demonstrate antibacterial properties, while larger quantities of iron oxides do not show any microbial activity.[39] All samples of the nanocomposite *C. spinosa* showed ZOI. The nanocomposite extracts demonstrated a significant inhibitory effect, especially in codes C and C1 at a dose of 100 mg/mL. Gram-positive in *Ba. cereus* has a ZOI of 16.7 mm in code C and 22.7 mm in code C1, whereas *Stap. aureus* has 20.1 mm in code C and 23.2 mm in code C1. The ZOI for gram-negative *Pseud. aeruginosa* is 17.7 mm in code C and 25 mm in code C1. Finally, *Kleb. pneumonia* has a code C ZOI of 15.7 mm and a C1 of 21.1 mm. Figures 10 and 11, exhibit these values. The data show that bacterial growth slows when Fe_3O_4-NP concentrations rise. Figures indicate the association between Fe_3O_4-NP concentration and ZOI for each nanocomposite extract. The ZOI difference between codes C and C1 is related to Fe_3O_4-NPs fabrication and IONP dimensions. Multiple effects come from alcoholic extracts targeting bacteria's hydrophilic and hydrophobic components. Alcohol extracts can solubilize a variety of compounds, making them effective against both gram-positive and gram-negative bacteria. Strong plant antimicrobial flavonoids and tannins are only soluble in alcohol or alcohol-water mixtures, increasing the extract's shelf life and potency. Pure and water-alcohol binary mixtures may extract antimicrobial flavonoids. As a solvent, alcohol may stabilise pH-dependent polyphenols such as flavonoids and tannins. This makes alcoholic extracts useful for extracting and preserving plant antibacterials.[40],[41] The exact mechanism responsible for the antibacterial effects of IONPs is still uncertain. However, certain investigations have indicated a connection with the generation of ROS.[42] ROS can potentially harm bacterial cells by oxidising their biological components, including DNA, lipids, and proteins. The concentration of IONPs in the culture medium directly influences the generation of ROS.[43] The antibacterial capabilities of IONPs are ascribed to their oxide concentration, size, shape, and other intrinsic physical and chemical features.[38] The effectiveness of IONPs in fighting against microbes has been demonstrated, although scientists are still studying the exact way in which they work.

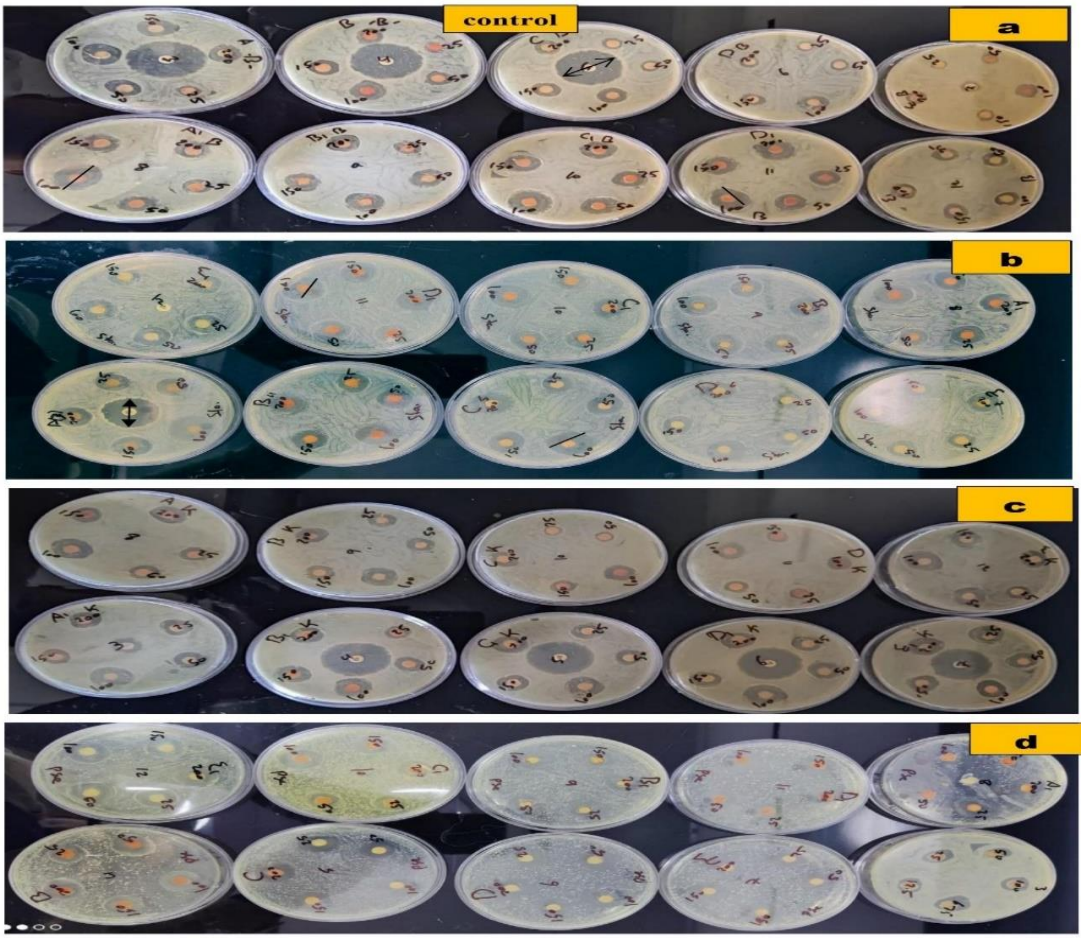

Figure 9: Inhibition zone images of (a) *Bacillus cereus,* (b) *Staphylococcus aureus*, (c) *Klebsiella pneumonia,* and (d) *Pseudomonas aeruginosa*

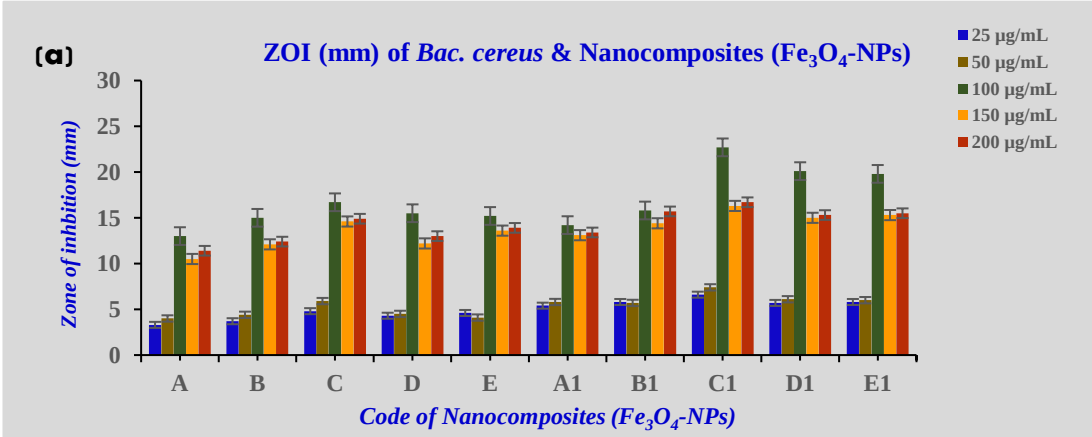

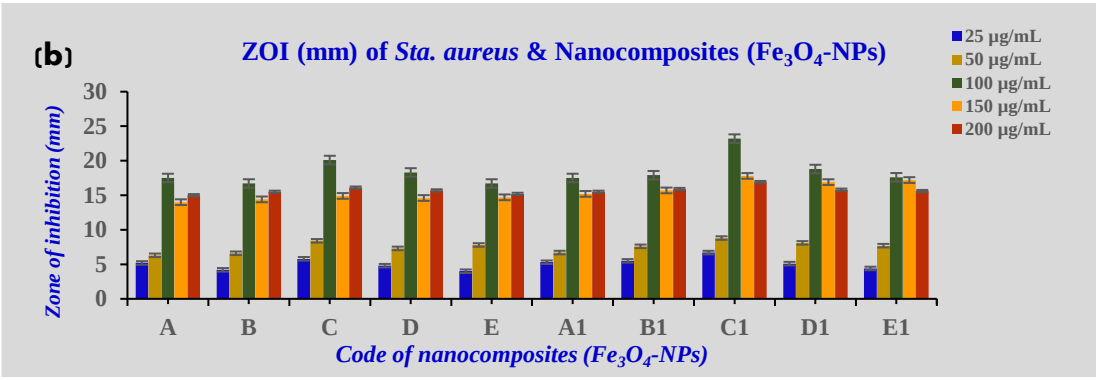

Figure 10: IOZ for (a) *Bacillus cereus* is (16.7 and 22.7 mm in codes C &C1, (b) *Staphylococcus aureus* is (20.1 and 23.2 mm in codes C by co-precipitation & C1 by green synthesis. (gram-positive)

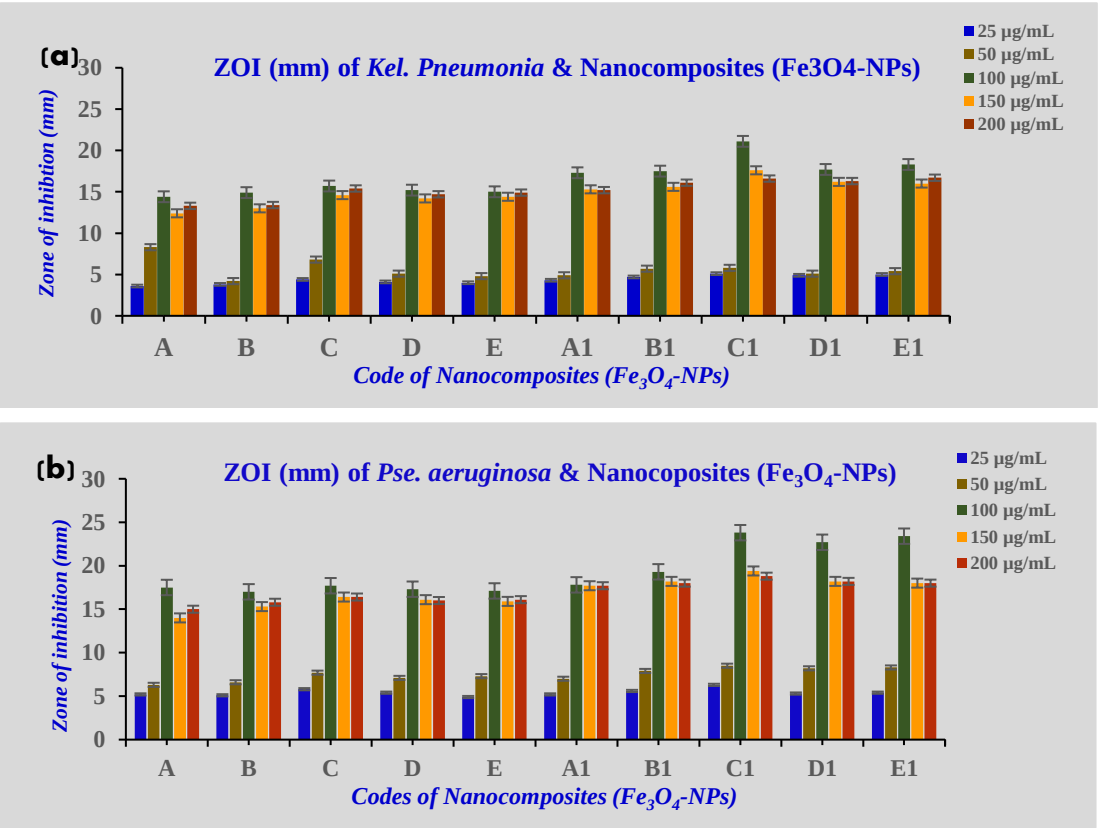

Figure 11: IOZ for (a) *Klebsiella Pneumoniae* is (15.7 and 21.1 mm in codes C &C1, (b) *Pseudomonas Aeruginosa* is (17.7 and 25 mm in codes C by co-precipitation & C1 by green synthesis. (gram-negative)

6. CONCLUSION

The study found that Fe_3O_4 NPs coated with extracts from *C. spinosa*, including aqueous, alcoholic, and alkaloids, demonstrated effective inhibition of two types of gram-positive bacteria (*Bacillus cereus* and *Staphylococcus aureus*) and two types of gram-negative bacteria (*Klebsiella pneumoniae* and *Pseudomonas aeruginosa*). Notably, the alcoholic extracts exhibited strong antibacterial properties against these bacteria. Each sample of the nanocomposite *C. spinosa* exhibited a Zone of Inhibition (ZOI). The nanocomposite extracts had a significant inhibitory impact, particularly in codes C and C1, when administered at a concentration of 100 mg/mL. Therefore, we recommend conducting more controlled experiments in living organisms to examine the efficacy of mouthwash in reducing streptococcal germs.

7. LIMITATIONS

Although this study offers useful insights into the antibacterial capabilities of Fe3O4-NPs coated with C. spinosa extracts, its scope is restricted to in vitro tests. Additional investigation is required to authenticate the efficacy of these nanocomposites in practical situations and to comprehend their potential adverse consequences. Moreover, the study did not investigate the complete range of microbial strains. Subsequent research could broaden the examination to include a wider variety of pathogens to assess the nanocomposites' antimicrobial effectiveness thoroughly.

8. RECOMMENDATIONS

Based on the results, it is advised to carry out more controlled tests, specifically in living creatures, to evaluate the effectiveness of the produced nanocomposites, particularly those coated with alcoholic extracts of C. spinosa, as possible antibacterial agents. Potential research endeavors may investigate the utilization of these nanocomposites in real-world scenarios, such as creating mouthwash formulas to counteract streptococcal bacteria. Furthermore, it is recommended to conduct further investigation into the durability, longevity, and real-world uses of the nanocomposites.

9. DECLARATIONS

Ethical Approval: The research conducted in this study was approved by the Ramadi Teaching Hospital for Maternity and the Consultative Clinic for Chest Diseases, ensuring compliance with ethical standards for human subject research.

Klebsiella pneumoniae bacteria were isolated from patients' sputum at the Ramadi Teaching Hospital for Maternity and the Consultative Clinic for Chest Diseases. This sample was subsequently transported to the laboratory for transplantation onto pre-prepared implants, whereas other bacteria were obtained from the soil.

Consent to Participate: All participants involved in this study provided informed consent before participating, indicating their voluntary participation in the research.

Consent to Publish: Participants have also consented to the publication of anonymized data gathered from the study, ensuring their confidentiality and privacy rights.

Authors Contributions: Each author's contribution to the manuscript is as follows: Majid A. Mohaisen's contributions, such as conceptualization, methodology, and writing, and Sirhan.M contributions, such as review & editing, etc.

Funding: The funding source had no role in the study design, data collection, analysis, interpretation, or writing of the manuscript.

Competing Interests: The authors declare that they have no competing interests that could influence the interpretation or presentation of the research findings.

Availability of data and materials: The data and materials used in this study are available upon request from the corresponding author, following institutional policies regarding data sharing and participant confidentiality.

By including these declarations, we aim to enhance the transparency and integrity of our research, providing readers and reviewers with the necessary information to evaluate and understand the study's methodology, findings, and implications.

References

1. Foschi ML, Juan M, Pascual B, Pascual-Seva N. Water uptake and germination of caper (Capparis spinosa L.) seeds. Agronomy. 2020;10(6):838. doi:10.3390/agronomy10060838.
2. Jiménez-López J, Ruiz-Medina A, Ortega-Barrales P, Llorent-Martínez EJ. Phytochemical profile and antioxidant activity of caper berries (Capparis spinosa L.): Evaluation of the influence of the fermentation process. Food Chem. 2018;250:54–59. doi:10.1016/j.foodchem.2018.01.010.
3. Zhao X, Liu W, Cai Z, Han B, Qian T, Zhao D. An overview of preparation and applications of stabilized zero-valent iron nanoparticles for soil and groundwater remediation. Water Res. 2016;100:245–266. doi:10.1016/j.watres.2016.05.019.
4. Ajitha B, Ashok Kumar Reddy Y, Reddy PS. Biogenic nano-scale silver particles by Tephrosia purpurea leaf extract and their inborn antimicrobial activity. Spectrochim. Acta - Part A Mol. Biomol. Spectrosc. 2014;121:164–172. doi:10.1016/j.saa.2013.10.077.
5. Ying S, et al. Green synthesis of nanoparticles: Current developments and limitations. Environ. Technol. Innov. 2022;26:102336. doi:10.1016/j.eti.2022.102336.
6. Shah M, Fawcett D, Sharma S, Tripathy SK, Poinern GEJ. Green synthesis of metallic nanoparticles via biological entities. 2015;8(11). doi:10.3390/ma8115377.
7. Castro L, Blázquez ML, Muñoz JA, González F, García-Balboa C, Ballester A. Biosynthesis of gold nanowires using sugar beet pulp. Process Biochem. 2011;46(5):1076–1082. doi:10.1016/j.procbio.2011.01.025.
8. Patra JK, Baek KH. Green Nanobiotechnology: Factors Affecting Synthesis and Characterization Techniques. J. Nanomater. 2014. doi:10.1155/2014/417305.
9. Akhtar MS, Swamy MK, Sinniah UR. Natural bio-active compounds. Nat. Bio-active Compd. Vol. 1 Prod. Appl. 2019. doi:10.1007/978-981-13-7154-7.
10. Aryee ANA, Boye JI. Current and Emerging and Manufacture of Functional Food Products. pp. 1–63.
11. Mariod HE, Tahir AA. Biological activities, definition, types and measurements. In: Multiple Biological Activities of Unconventional Seed Oils. 2022. pp. 17–28.

12. Ansari SA, et al. Antibacterial activity of iron oxide nanoparticles synthesized by co-precipitation technology against Bacillus cereus and Klebsiella pneumoniae. Polish J. Chem. Technol. 2017;19(4):110–115. doi:10.1515/pjct-2017-0076.
13. You A, Be MAY, In I. Green synthesis of zinc oxide nanoparticles using leaves extract of capparis for adsorption of nickel (II) and copper (II) ions. 2023;040010(March). doi:10.1016/j.eti.2022.102336.
14. Der Duh P, Yen GC. Antioxidative activity of three herbal water extracts. Food Chem. 1997;60(4):639–645. doi:10.1016/S0308-8146(97)00049-6.
15. Zhou X, Peng J, G. Fan, Wu Y. Isolation and purification of flavonoid glycosides from Trollius ledebouri using high-speed counter-current chromatography by stepwise increasing the flow-rate of the mobile phase. J. Chromatogr. A. 2005;1092(2):216–221. doi:10.1016/j.chroma.2005.07.064.
16. Doncheva T, Berkov S, Philipov S. Comparative study of the alkaloids in tribe Datureae and their chemosystematic significance. Biochem. Syst. Ecol. 2006;34(6):478–488. doi:10.1016/j.bse.2006.01.008.
17. Gao M, Li W, Dong J, Zhang Z, Yang B. Synthesis and Characterization of Superparamagnetic Fe3O4@SiO2 Core-Shell Composite Nanoparticles. World J. Condens. Matter Phys. 2011;1(1):49–54. Available at: http://www.scirp.org/journal/wjcmp.
18. Wang Z, Guo J, Ma J, Shao L. Highly regenerable alkali-resistant magnetic nanoparticles inspired by mussels for rapid selective dye removal offer high-efficiency environmental remediation. J. Mater. Chem. A. 2015;3(39):19960–19968. doi:10.1039/c5ta04840k.
19. Kanagasubbulakshmi S, Kadirvelu K. Green synthesis of Iron oxide nanoparticles using Lagenaria siceraria and evaluation of its Antimicrobial activity. Def. Life Sci. J. 2017;2(4):422. doi:10.14429/dlsj.2.12277.
20. Shnoudeh AJ, et al. Synthesis, Characterization, and Applications of Metal Nanoparticles. Elsevier Inc.; 2019. doi:10.1016/B978-0-12-814427-5.00015-9.
21. Razmavar S, Abdulla MA, Ismail SB, Hassandarvish P. Antibacterial activity of leaf extracts of Baeckea frutescens against methicillin-resistant Staphylococcus aureus. Biomed Res. Int. 2014;2014. doi:10.1155/2014/521287.
22. Tendencia EA. Chapter 2. Disk diffusion method. In: Lab. Man. Stand. methods Antimicrob. Sensit. tests Bact. Isol. from Aquat. Anim. Environ. 2004. pp. 13–29.
23. Bhargav HS, Shastri SD, Poornav SP, Darshan KM, Nayak MM. Measurement of the Zone of Inhibition of an Antibiotic. Proc. - 6th Int. Adv. Comput. Conf. IACC 2016. 2016;409–414. doi:10.1109/IACC.2016.82.
24. Fajaroh F, Setyawan H, Widiyastuti W, Winardi S. Synthesis of magnetite nanoparticles by surfactant-free electrochemical method in an aqueous system. Adv. Powder Technol. 2012;23(3):328–333. doi:10.1016/j.apt.2011.04.007.
25. Hoseini SJ, Nasrabadi H, Azizi M, Beni AS, Khalifeh R. ChemInform Abstract: Fe3O4 Nanoparticles as an Efficient and Magnetically Recoverable Catalyst for Friedel-Crafts Acylation Reaction in Solvent-Free Conditions. ChemInform. 2013;44(31):no-no. doi:10.1002/chin.201331073.
26. Demir A, Topkaya R, Baykal A. Green synthesis of superparamagnetic Fe3O4 nanoparticles with maltose: Its magnetic investigation. Polyhedron. 2013;65:282–287. doi:10.1016/j.poly.2013.08.041.
27. Yang K, Peng H, Wen Y, Li N. Re-examination of characteristic FTIR spectrum of secondary layer in bilayer oleic acid-coated Fe3O4 nanoparticles. Appl. Surf. Sci. 2010;256(10):3093–3097. doi:10.1016/j.apsusc.2009.11.079.
28. Mahdavi M, Namvar F, Bin Ahmad M, Mohamad R. Green biosynthesis and characterization of magnetic iron oxide (Fe3O4) nanoparticles using seaweed (Sargassum muticum) aqueous extract. Molecules. 2013;18(5):5954–5964. doi:10.3390/molecules18055954.

29. Alterary SS, Alkhamees A. Synthesis, surface modification, and characterization of Fe3O4@SiO2 core@shell nanostructure. Green Process. Synth. 2021;10(1):384–391. doi:10.1515/gps-2021-0031.
30. Ahghari MR, Amiri-khamakani Z, Maleki A. Synthesis and characterization of Se doped Fe3O4 nanoparticles for catalytic and biological properties. Sci. Rep. 2023;13(1):1–14. doi:10.1038/s41598-023-28284-x.
31. Ba-Abbad MM, Benamour A, Ewis D, Mohammad AW, Mahmoudi E. Synthesis of Fe3O4 Nanoparticles with Different Shapes Through a Co-Precipitation Method and Their Application. Jom. 2022;74(9):3531–3539. doi:10.1007/s11837-022-05380-3.
32. Bagtash M, Yamini Y, Tahmasebi E, Zolgharnein J, Dalirnasab Z. Magnetite nanoparticles coated with tannic acid as a viable sorbent for solid-phase extraction of Cd2+, Co2+, and Cr3+. Microchim. Acta. 2016;183(1):449–456. doi:10.1007/s00604-015-1667-5.
33. Wang Q, Snyder S, Kim J, Choi H. Aqueous ethanol modified nanoscale zerovalent iron in Bromate reduction: Synthesis, characterization, and reactivity. Environ. Sci. Technol. 2009;43(9):3292–3299. doi:10.1021/es803540b.
34. Wang LS, Hong RY. Synthesis, Surface Modification and Characterisation of Nanoparticles. Adv. Nanocomposites - Synth. Charact. Ind. Appl. 2011. doi:10.5772/10540.
35. Fathima JB, Pugazhendhi A, Oves M, Venis R. Synthesis of eco-friendly copper nanoparticles for augmentation of catalytic degradation of organic dyes. J. Mol. Liq. 2018;260:1–8. doi:10.1016/j.molliq.2018.03.033.
36. Khodabakhshi S, Karami B, Eskandari K, Hoseini SJ, Nasrabadi H. Convenient on water synthesis of novel derivatives of dicoumarol as functional vitamin K depleter by Fe3O4 magnetic nanoparticles. Arab. J. Chem. 2017;10:S3907–S3912. doi:10.1016/j.arabjc.2014.05.030.
37. Mahdavi M, Bin Ahmad M, Haron MJ, Gharayebi Y, Shameli K, Nadi B. Fabrication and Characterization of SiO2/(3-Aminopropyl)triethoxysilane-Coated Magnetite Nanoparticles for Lead(II) Removal from Aqueous Solution. J. Inorg. Organomet. Polym. Mater. 2013;23(3):599–607. doi:10.1007/s10904-013-9820-2.
38. Gudkov SV, Burmistrov DE, Serov DA, Rebezov MB, Semenova AA, Lisitsyn AB. Do iron oxide nanoparticles have significant antibacterial properties? Antibiotics. 2021;10(7):1–23. doi:10.3390/antibiotics10070884.
39. Ezealigo US, Ezealigo BN, Aisida SO, Ezema FI. Iron oxide nanoparticles in biological systems: Antibacterial and toxicology perspective. JCIS Open. 2021;4(July):100027. doi:10.1016/j.jciso.2021.100027.
40. Noveiri P, Rezvaninejad R, Azarm A, Rezvaninejad R. Antibacterial effects of aqueous and alcoholic extracts of Zataria multiflora in comparison with chlorhexidine mouthwash on some pathogenic oral streptococci: An in vitro study. Dent. Res. J. (Isfahan). 2023;20(1):48. doi:10.4103/1735-3327.374805.
41. Chaves JO, et al. Extraction of Flavonoids From Natural Sources Using Modern Techniques. Front. Chem. 2020;8(September). doi:10.3389/fchem.2020.507887.
42. Abdulsada FM, Hussein NN, Sulaiman GM, Al Ali A, Alhujaily M. Evaluation of the Antibacterial Properties of Iron Oxide, Polyethylene Glycol, and Gentamicin Conjugated Nanoparticles against Some Multidrug-Resistant Bacteria. J. Funct. Biomater. 2022;13(3). doi:10.3390/jfb13030138.
43. Arakha M, et al. Antimicrobial activity of iron oxide nanoparticle upon modulation of nanoparticle-bacteria interface. Sci. Rep. 2015;5:1–12. doi:10.1038/srep14813.